THE JOURNAL OF PHYSICAL CHEMISTRY C

Article

pubs.acs.org/JPCC

Surface and Internal Reactions of ZnO Nanowires: Etching and Bulk Defect Passivation by H Atoms

Wooseok Kim,[†,∥] Geunjae Kwak,[†,∥] Minbok Jung,[‡] Sam K. Jo,[‡] James B. Miller,[§] Andrew J. Gellman,[§] and Kijung Yong*,[†]

[†]Surface Chemistry Laboratory of Electronic Materials, Department of Chemical Engineering, Pohang University of Science and Technology (POSTECH), Pohang 790-784, South Korea

[‡]Department of Chemistry, Gachon University, Sungnam, Kyungki 461-701, South Korea

[§]Department of Chemical Engineering, Carnegie Mellon University, Pittsburgh, Pennsylvania 15213, United States

ABSTRACT: Reactions of ZnO nanowires (NWs) with atomic hydrogen were investigated with temperature-programmed desorption (TPD) mass spectrometry, scanning electron microscopy, and photoluminescence (PL) spectroscopy. During TPD, molecular H_2, H_2O, and atomic Zn desorbed from ZnO NWs pretreated with atomic H at 220 K. Three distinct H_2 TPD peaks, two from surface H states and one from a bulk H state, were identified. The TPD assignment of the bulk H state was corroborated by significantly suppressed emission at 564 nm and enhanced emission at 375 nm in PL experiments. Etching of ZnO NWs by atomic H was confirmed by desorption of molecular H_2O and atomic Zn in TPD and by electron microscopic images of H-treated ZnO NWs. A mechanistic model for underlying H/ZnO NW reactions is proposed and discussed.

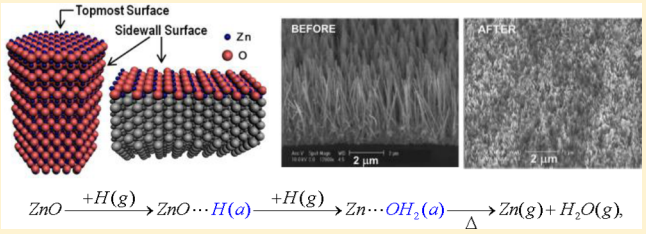

1. INTRODUCTION

Zinc oxide (ZnO), an n-type compound semiconductor with a wide direct band gap (3.4 eV) and a large exciton binding energy (60 meV), has been widely studied because of its unique electrical, optoelectronic, piezoelectric, and catalytic properties.[1−3] As reported by Van de Walle and his colleagues, the intrinsic n-type conductivity of undoped ZnO is due to the incorporation of interstitial hydrogen into the ZnO structure.[4] According to their theoretical model, interstitial hydrogen acts as a shallow donor, effectively functioning as an n-type dopant. Recent studies have reported that hydrogen can improve carrier mobility, increase electrical conductivity, and even alter magnetic properties of doped ZnO. In addition, hydrogenation improves photoluminescence (PL) by both decreasing deep level emission and increasing band-edge emission.[5]

Hydrogen's interactions with ZnO have been widely investigated to elucidate the underlying mechanisms and impact on ZnO properties. In particular, interactions of hydrogen with specific single-crystalline ZnO surfaces [polar $(0001)/(000\bar{1})$ and nonpolar $(10\bar{1}0)$] have been studied by a variety of methods.[6−13] These studies show that the adsorption and reactivity of hydrogen vary widely, sensitively depending on the facet, the atomic structure, of ZnO surfaces. In addition, the penetration of hydrogen into the subsurface of ZnO and its subsequent interstitial migration (diffusion) in the crystalline ZnO bulk have also been suggested by several studies.[14−18] However, despite these studies, the detailed reaction mechanism(s) and the role of surface atomic structure in the hydrogenation of ZnO remain uncertain.

Recently, one-dimensional (1D) ZnO nanostructures have attracted interest as building blocks for fabricating nanodevices such as field effect transistors (FET),[19] chemical sensors,[20] light-emitting diodes (LED),[21] and solar cells.[22] ZnO nanowires (NWs) have large surface-area-to-volume ratios; thus, surface properties can determine their performance in these applications. The understanding of hydrogen reactions with the surface and bulk of ZnO NWs is of crucial importance to their application in future devices. In this work, we report the results of our detailed experimental characterization of the reactions of hydrogen with ZnO NWs; our results will enable fundamental understanding and optimization of ZnO-based nanodevices.

ZnO NWs grow preferentially along the *c*-axis of their wurtzite crystal structure. A highly crystalline ZnO NW has a structure with a hexagonal cross section; the exposed surfaces of a ZnO NW consist of a top face (normal to the *c*-axis) and side-wall faces (parallel to the *c*-axis). Due to the high aspect ratio of the NW, the total area of side walls is much greater than that of the top face. The side walls of a ZnO NW present equal densities of Zn^{2+} and O^{2-} ions, so the polarity of each ion is offset. This means that the majority of the exposed surfaces of a ZnO NW are nonpolar. As a result, in the case of ZnO NWs, chemical reactions on nonpolar surfaces are expected to be dominant.

In this work, we have investigated hydrogen reactions with hydrothermally grown ZnO NW arrays in an ultrahigh vacuum

Received: May 1, 2012
Revised: July 6, 2012
Published: July 12, 2012

 © 2012 American Chemical Society dx.doi.org/10.1021/jp304191m | J. Phys. Chem. C 2012, 116, 16093−16097

(UHV) system. Temperature-programmed desorption (TPD) was used to study the reaction of atomic hydrogen with ZnO NWs. From ZnO NWs exposed to atomic hydrogen at a temperature below 200 K, we have detected desorption of various reaction products, including molecular hydrogen, water, and metallic Zn in subsequent TPDs. Mulitple desorption peaks of molecular hydrogen imply a variety of binding states of atomic H on ZnO NWs. We have also observed desorption of metallic Zn and H_2O from ZnO NW surfaces exposed to atomic H as a result of H-induced etching, which was confirmed by microscopic analyses of samples after TPD experiments. On the basis of these findings, a reaction mechanism of atomic hydrogen on ZnO NWs is proposed and discussed.

2. EXPERIMENTAL SECTION

A 4 in. diameter p-type (1−10 Ω cm) Si(100) wafer was cleaned with HF and sequentially sputter coated with 200 Å Ta and 2000 Å W on its reverse side. A ∼50 nm thick ZnO layer was deposited on the Si substrate to act as a seed layer for the NWs. ZnO NW arrays were then grown on the seed layer by an ammonia-solution method that we previously described.[23] Experiments were carried out in a turbomolecular-pumped ultrahigh vacuum (UHV) system with a base pressure of 4.5×10^{-11} Torr. A main 500 L/s turbo pump was backed by a 50 L/s oil diffusion and a mechanical pump, in series. Samples of ZnO NW arrays grown on Si(100) were diced to 10×20 mm^2 and mounted on an *XYZ*-rotational manipulation stage in the UHV chamber. The sample manipulator has provisions for LN_2 sample cooling, electrical feed throughs for dc-resistive sample heating, and a type K thermocouple inserted and glued (Aremco 516 high-temperature ceramic adhesive) into a small hole drilled on the sample edge for accurate temperature measurements. The sample temperature was regulated precisely by a dc power supply, which is in turn controlled by an electronic temperature programmer interfaced to PC control software.

The UHV chamber was also equipped with (a) a differentially pumped triple-filter quadrupole mass spectrometer (QMS, Thermo Scientific Smart IQ+ model) for residual gas analysis (RGA) and temperature-programmed desorption (TPD) measurements of desorbing species from the sample, (b) a high-purity gas delivery system with a tubular dual-gas doser with a precision leak valve, and (c) a spiral hot (∼1900 K) tungsten filament for cracking H_2 molecules into H atoms.

Because of the unknown thermal dissociation efficiency of H_2 gas molecules, all H-atom exposures are reported with those of molecular H_2 measured in Langmuirs (1 L = 1×10^{-6} Torr s). After each H-atom dose of a given exposure, the sample was rotated 90° away from the tubular gas doser and positioned in front of a 3 mm-diameter aperture cone to face the differentially pumped QMS from a line-of-sight distance of ∼1 mm for TPD measurements. The small distance suppresses signal contributions from background sources. The ultrahigh-purity (99.999%) H_2 gas was purified with an LN_2 trap in a baked and turbo-pumped gas manifold and checked for impurities with the RGA before introduction to the sample surface. The sample can be heated to 970 K and cooled below 100 K. After gas exposure at a given surface temperature (T_s), TPD spectra were acquired as the sample was heated at a rate of 2.5 K/s.

3. RESULTS AND DISCUSSION

For our study of surface reactions with atomic H, ZnO NW array samples were prepared by a hydrothermal technique. Figure 1a shows a cross-sectional scanning electron microscope

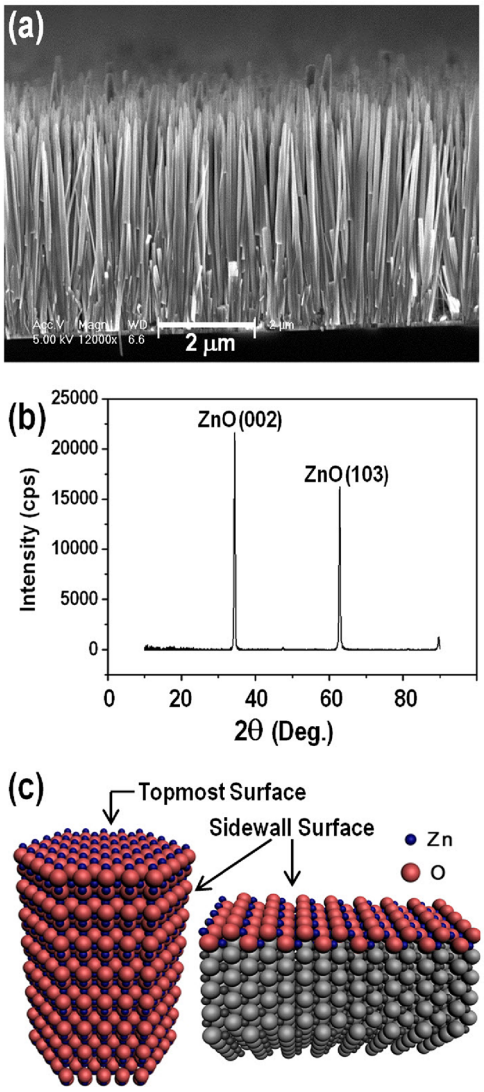

Figure 1. (a) SEM image of ZnO NWs fabricated by a hydrothermal method. (b) XRD spectra of the hydrothermally grown ZnO NWs. (c) Schematic diagrams of a single-crystalline ZnO NW, grown along the *c*-axis, with its Zn polar topmost surface (left) and nonpolar side-wall face with alternating rows of Zn and O atoms exposed on the surface (right).

(SEM) image of an array of ZnO NWs. NWs are, on average, 4 μm long and 100 nm thick. We characterized the crystalline order of the ZnO NWs by X-ray diffraction (XRD, 2θ scan). As shown in Figure 1b, there are two prominent XRD peaks, which are attributed to ZnO(103) of the underlying seed layer and ZnO(002) of the NWs grown vertically along the *c*-axis of the crystal plane. These XRD results indicate that our ZnO NWs are highly crystalline. Figure 1c schematically shows the hexagonal crystal structure of our ZnO NW. The topmost face of the single-crystalline ZnO NW is terminated by Zn^{2+} ions (polar surface), while the side-wall faces are exposed by both Zn^{2+} and O^{2-} ions (nonpolar surface).

To probe the interactions of hydrogen with the ZnO NWs, we adsorbed molecular H_2 onto the ZnO NWs, over a range of exposures, at a sample temperature of 120 K, and then monitored desorption/reaction products by mass spectrometry during a linear temperature ramp to 900 K. The only desorbing species observed was molecular H_2 (which desorbed below 300 K), indicating that hydrogen is bound weakly on ZnO NWs, in agreement with a literature report.[25]

To enhance the reactivity of ZnO NWs toward hydrogen, the NWs were dosed with atomic hydrogen. Thermal cracking of molecular H_2 with a hot tungsten filament was employed to generate thermal-energy H atoms (cracking percentage is 5−10%). By varying the H-atom dose from 50 to 10^6 L (measured as H_2 exposures), we examined the reaction products by carrying out TPD measurements, detecting H_2, H_2O, and atomic Zn from our ZnO NW samples pretreated with atomic H. Figure 2a presents the coverage-dependent H_2 (m/z = 2) desorption spectra obtained from ZnO NWs pretreated with H atoms at 220 K. H_2 desorption was observed over a broad temperature range, 250−700 K. The total amount of H_2 desorption grew with increasing exposure until saturation occurred at ∼5 × 10^5 L. The broad, irregular desorption curve is suggestive of multiple adsorption states. To discern states of different adsorption energies, we fit three Gaussian peaks to the 1 × 10^6 L TPD curve. Figure 2b shows the result, exhibiting peaks at 330, 450, and 553 K.

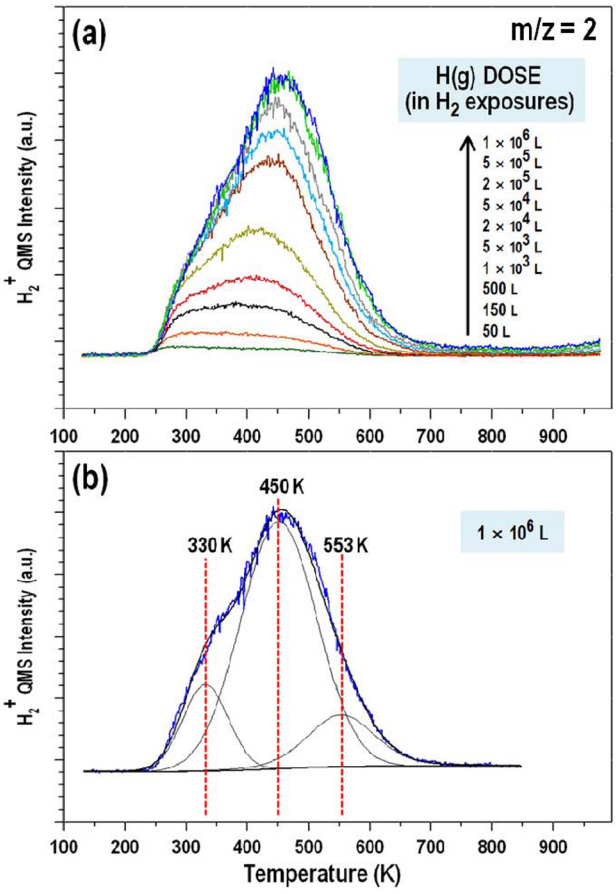

Figure 2. (a) Series of TPD spectra of molecular H_2 (m/z = 2) from ZnO NWs pre-exposed to increasing atomic H(g) doses at a substrate temperature of 220 K. (b) Saturation H_2 TPD peak and three deconvoluted peaks.

Our observation of three component peaks implies three binding states of atomic H on ZnO NWs; this is in contrast with most literature reports of two H_2-desorption features from single-crystalline ZnO surfaces, in which low- and high-temperature peaks are ascribed to Zn−H and O−H or bulk desorption, respectively.[6,8,11] Considering unique atomic structure of our ZnO NWs as shown in Figure 1c, it is not surprising that the interaction of atomic hydrogen with ZnO NWs is more complicated than that with a single-crystalline surface.

To further understand the origin of each desorption feature, we inspected the growth behaviors of desorption peaks. At low exposures, only the two low-temperature peaks were observed. We ascribe these two peaks to two distinguished H adsorption states on the surface of our ZnO NWs. As shown in Figure 1c, our crystalline ZnO NWs consist of two distinct surfaces: the topmost Zn-terminated polar and nonpolar side-wall faces. Because the side-wall faces have a far larger total surface area than the terminal polar faces, they will dominate the surface chemistry of the ZnO NWs. The nonpolar side-wall faces present equal densities of Zn^{2+} and O^{2-} surface ions as sites for H adsorption. Atomic H is expected to adsorb on both of these two sites, forming Zn−H or O−H bonds.

When exposed to atomic H at 220 K, both Zn and O sites on our ZnO NW surfaces would be occupied by adsorbed H (ZnO−2H). Adsorbed H atoms, Zn−H(a) and O−H(a), on ZnO NW surfaces would desorb molecularly as H_2 at two different temperatures, 330 and 450 K, respectively, reflecting their adsorption strengths, as shown in Figure 2. The more strongly bound H atoms on the surface oxygen are removed completely when heated to 685 K, restoring the clean ZnO surface.[11] Similarly, Chan and Griffin[26] reported that adsorbed H(a) desorbed from Zn sites at ∼319 K, in good agreement with our results and peak assignments. A He-diffraction study of H/ZnO(10−10)[11] also revealed that all O−H adsorption states were removed at 685 K, which further supports our peak assignments.

We now turn to the component H_2 desorption peak at 553 K, apparent only at high H-atom exposures beyond 1000 L (see Figure 2). Hydrogen absorption by and diffusion into crystalline ZnO have been documented both experimentally and theoretically. Recently, Doh et al. reported that H atoms absorbed by ZnO single crystals desorbed at ∼539 K.[8] Their 539 K H_2 desorption peak, assigned to bulk-absorbed H, was observed only at high H(g) atom exposures, in agreement with our results. However, in contrast to their result, our 553 K H_2 peak is saturated. We attribute this to our NW-structured ZnO sample, which would have a finite volume for H absorption unlike a ZnO single crystal sample. Jung et al. reported similar results, that is, saturation and even apparent suppression of H absorption by their heavily HF-etched Si(100) samples.[28] It should also be noted that the 553 K bulk H peak grows at a slower rate than the 330 and 450 K surface H peaks, as previously reported.[29]

Hydrogen is known to strongly affect the PL of ZnO nanomaterials. In Figure 3a, our as-grown ZnO NWs exhibit a broad deep-level emission (DLE) at ∼564 nm.[5] This yellow emission is generally attributed to excess oxygen, common in ZnO NWs grown in aqueous solutions.[24] One important aspect is that this 564 nm emission is quenched completely while the near band-edge emission (NBE) is greatly enhanced at 375 nm when H atoms are incorporated into ZnO NWs by thermal annealing in an H_2 ambient atmosphere above 300 °C. This

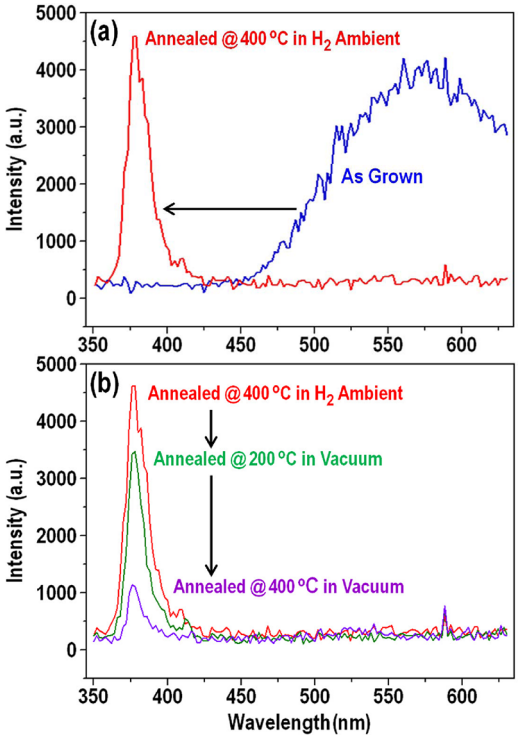

Figure 3. (a) PL scans of our sample of ZnO NWs as grown (blue) and treated in H_2 ambient at 400 °C (red). (b) PL spectra of the NWs annealed in an H_2 ambient atmosphere initially at 400 °C (red) and then by vacuum annealing at 200 °C (green) and 400 °C (purple).

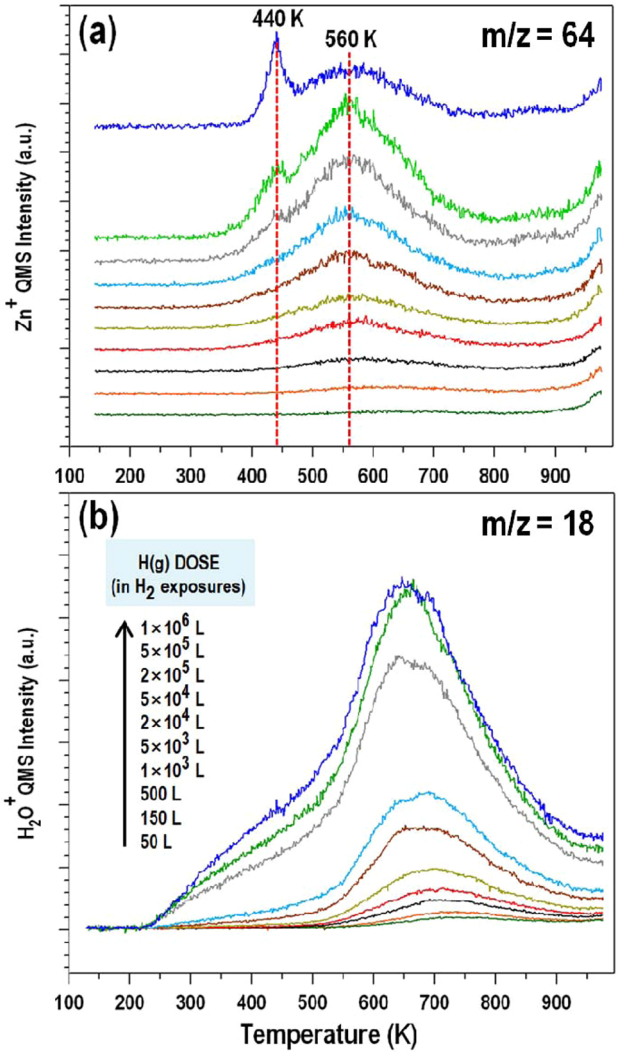

Figure 4. (a) TPD spectra of zinc (m/z = 64). (b) Water (m/z = 18) from ZnO NWs pre-exposed to various doses of atomic H(g) at 220 K.

indicates that absorbed H atoms efficiently annihilate defects in ZnO NWs. We thus conclude that the DLE peak is suppressed due to the defect passivation by H, while the strong NBE peak is attributed to the increase in electron density by incorporated H. To examine the effect of removal of absorbed H on the PL properties, we annealed our H-treated ZnO NW samples in vacuum. Figure 3b depicts the PL spectra of our hydrogen-pretreated ZnO NW sample as a function of the temperature of postannealing in a vacuum. While annealing at 200 °C decreased the NBE peak intensity slightly, annealing at 400 °C dramatically suppressed the NBE without any DLE, which we ascribe to the desorption of absorbed H from ZnO NWs as shown in Figure 2. This result indicates that the bulk-absorbed hydrogen plays a crucial role in the passivation of defects in ZnO NWs.

In addition to molecular H_2, other reaction products, water (m/z = 18) and zinc (m/z = 64), desorbed during TPD from H-dosed ZnO NWs. As shown in Figure 4a, Zn desorbs broadly at 560 K and, in addition, sharply at 440 K with increasing H(g) doses. ZnO etching by atomic H(g) was proposed by Bruno et al. on the basis of their theoretical calculations and AFM measurements.[13] In their model, atomic H breaks Zn−O bonds to form either metallic Zn or zinc hydrides ZnH_x, depending on the surface atomic structure of ZnO. In accordance with their model, zinc hydrides form as a result of H-atom reactions with nonpolar surfaces of ZnO. ZnH_x species are known to desorb at a relatively low temperature of 380 K. However, no desorption of ZnH_x occurred, but metallic Zn was detected in our TPDs. This was inconsistent with their nonpolar ZnO surface model. Wöll et al. proposed a similar model in which the adsorption of H atoms on ZnO(10−10) induces formation of defects, resulting in H_2O formation and ZnO etching.[27] We now propose the following reaction mechanism from our results:

$$\mathrm{ZnO} \xrightarrow{+\mathrm{H(g)}} \mathrm{ZnO{\cdots}H(a)}$$
$$\xrightarrow{+\mathrm{H(g)}} \mathrm{Zn{\cdots}OH_2(a)}$$
$$\underset{\Delta}{\rightarrow} \mathrm{Zn(g) + H_2O(g)}$$

where (g) and (a) stand for gaseous and adsorbed, respectively.

In this model, gas-phase H atoms react with ZnO in two steps: (1) an H(g) atom adsorbs on the O atom site, and (2) an additional H(g) atom now attacks the surface O atom with a preadsorbed H(a) atom and breaks the Zn−O bond, forming an adsorbed H_2O molecule and a reduced Zn atom on the surface. This H_2O(a) molecule and reduced Zn atoms are believed to desorb molecularly and atomically, respectively, during TPD, in agreement with our experimental results. Moreover, an excessively high H-atom dose would create an agglomeration of excess Zn atoms (i.e., metallic Zn), which would desorb at an even lower temperature, as detected by a low-temperature shoulder peak at 440 K in Figure 4a. Water, another reaction product, also desorbs from OH groups on the

surface as shown in Figure 4b. Surface-adsorbed H(a) would desorb as either molecular H_2 or H_2O via the Zn−O bond breakage during TPD. Our results suggest that these two reactions compete.

Etching ZnO NWs by atomic H(g) was confirmed also by SEM analyses. Figure 5 shows SEM images of ZnO NWs before and after repeated H-dose/TPD experiments. As can be seen, the initially well-aligned ZnO NWs are etched out and only the bottom parts of NWs remain. A deposition of metallic Zn could be seen on the outer surface of our cone-shaped QMS skimmer, which faces the sample surface from a 1 mm distance during TPDs. All of these results clearly indicate etching of ZnO NWs by atomic H(g). We conclude that, while the etching of a single-crystalline ZnO surface by H(g) is difficult to achieve, the high surface-to-volume ratio due to our nanowire ZnO structure enables H(g)-induced etching of our ZnO NWs, even at low temperatures. Although we believe that the etching reaction occurs dominantly on nonpolar side walls of ZnO NWs, we cannot rule out that some etching occurred on the Zn-terminated topmost surface of NWs.

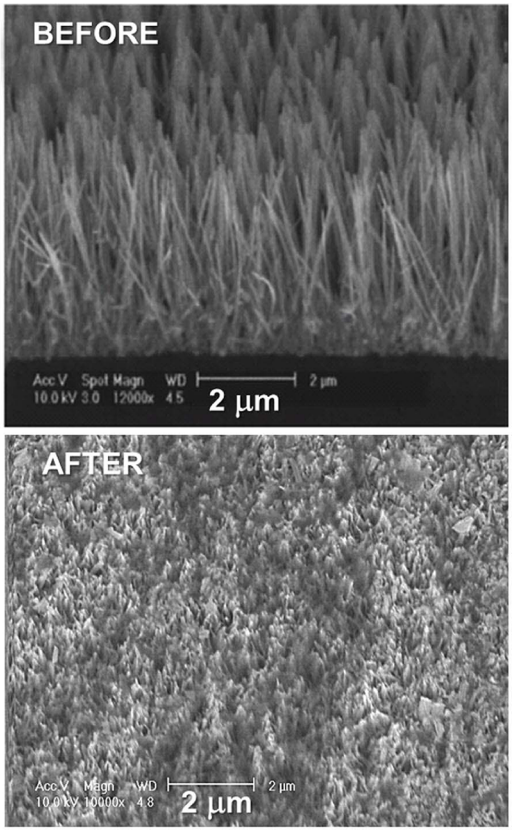

Figure 5. SEM images of ZnO NWs before (top) and after (bottom) repeated H(g) atom doses/TPDs.

4. CONCLUSION

We have investigated reactions between H(g) atoms and hydrothermally grown ZnO NWs. Three distinct H_2 desorption states at 330, 450, and 553 K were attributed to chemisorbed H(a) on Zn and O sites on nonpolar side-wall surfaces of ZnO NWs and H absorbed by the ZnO bulk, respectively. Surface etching products, H_2O and metallic Zn, also desorbed as a result of the Zn−O surface bond breaking during TPD. A mechanistic model for etching and bulk absorption has been proposed and discussed.

■ AUTHOR INFORMATION

Corresponding Author

*E-mail: kyong@postech.ac.kr. Phone: +82-54-279-2278.

Author Contributions

[‖]Equally contributed.

Notes

The authors declare no competing financial interest.

■ ACKNOWLEDGMENTS

This work was supported by the 2011 Global Research Network Program (220-2011-1-C00033). S.K.J. acknowledges a National Research Foundation of Korea grant, funded by the Korean government (NRF-MEST Grant 2012-0000905).

■ REFERENCES

(1) Klingshirn, C. *ChemPhysChem* **2007**, *8*, 782.
(2) Wang, Z. L. *Appl. Phys. A: Mater. Sci. Process.* **2007**, *88*, 7.
(3) Behnajady, M. A.; Modirshahla, N.; Hamzavi, R. *J. Hazard. Mater.* **2006**, *133*, 226.
(4) Van de Walle, C. G. *Phys. Rev. Lett.* **2000**, *85*, 1012.
(5) Tak, Y.; Park, D.; Yong, K. *J. Vac. Sci. Technol., B: Microelectron. Nanometer Struct.—Process., Meas., Phenom.* **2006**, *24*, 2047.
(6) Becker, T.; Hövel, S.; Kunat, M.; Boas, C.; Burghaus, U.; Wöll, C. *Surf. Sci.* **2001**, *486*, L502.
(7) Meyer, B. *Phys. Rev. B* **2004**, *69*, 045416.
(8) Doh, W. H.; Roy, P. C.; Kim, C. M. *Langmuir* **2010**, *26*, 16278.
(9) Zapol, P.; Jaffe, J. B.; Hess, A. C. *Surf. Sci.* **1999**, *422*, 1.
(10) Wander, A.; Harrison, N. M. *J. Phys. Chem. B* **2001**, *105*, 6191.
(11) Wang, Y.; Meyer, B.; Yin, X.; Kunat, M.; Langenberg, D.; Traeger, F.; Birkner, A.; Wöll, C. *Phys. Rev. Lett.* **2005**, *95*, 266104.
(12) Yin, X.-L.; Birkner, A.; Hanel, K.; Lober, T.; Kohler, U.; Woll, C. *Phys. Chem. Chem. Phys.* **2006**, *8*, 1477.
(13) Bruno, G.; Giangregorio, M. M.; Malandrino, G.; Capezzuto, P.; Fragalà, I. L.; Losurdo, M. *Adv. Mater.* **2009**, *21*, 1700.
(14) Wardle, M. G.; Goss, J. P.; Briddon, P. R. *Phys. Rev. Lett.* **2006**, *96*, 205504.
(15) Ip, K.; Overberg, M. E.; Heo, Y. W.; Norton, D. P.; Pearton, S. J.; Stutz, C. E.; Luo, B.; Ren, F.; Look, D. C.; Zavada, J. M. *Appl. Phys. Lett.* **2003**, *82*, 385.
(16) Janotti, A.; Van de Walle, C. G. *Nat. Mater.* **2007**, *6*, 44.
(17) Bang, J.; Chang, K. J. *Appl. Phys. Lett.* **2008**, *92*, 132109.
(18) Nickel, N. H. *Phys. Rev. B: Condens. Matter Mater. Phys.* **2006**, *73*, 195204.
(19) Goldberger, J.; Sirbuly, D. J.; Law, M.; Yang, P. *J. Phys. Chem. B* **2005**, *109*, 9.
(20) Wan, Q.; Li, Q. H.; Chen, Y. J.; Wang, T. H.; He, X. L.; Li, J. P.; Lin, C. L. *Appl. Phys. Lett.* **2004**, *84*, 3654.
(21) Bao, J.; Zimmler, M. A.; Capasso, F.; Wang, X.; Ren, Z. F. *Nano Lett.* **2006**, *6*, 1719.
(22) Law, M.; Greene, L. E.; Johnson, J. C.; Saykally, R.; Yang, P. *Nat. Mater.* **2005**, *4*, 455.
(23) Tak, Y.; Yong, K. *J. Phys. Chem. B* **2005**, *109*, 19263.
(24) Djurišić, A. B.; Leung, Y. H. *Small* **2006**, *2*, 944.
(25) Griffin, G.; Yates, J., Jr. *J. Chem. Phys.* **1982**, *77*, 3751.
(26) Chan, L.; Griffin, G. L. *Surf. Sci.* **1984**, *145*, 185.
(27) Woll, C. *Prog. Surf. Sci.* **2007**, *82*, 55.
(28) Jung, M.; Jo, S. K. *J. Phys. Chem. C* **2011**, *115*, 23463.
(29) Jo, S. K.; Kang, J. H.; Yan, X.-M.; White, J. M.; Ekerdt, J. G.; Keto, J. W.; Lee, J. *Phys. Rev. Lett.* **2000**, *79*, 36.